Article

Discovery Medicine 2024; 36(186): 1499–1512
https://doi.org/10.24976/Discov.Med.202436186.139

Local Anesthetic Bupivacaine Inhibits Melanoma Proliferation and Metastasis by Targeting PAPSS2

Enjian Guan[1], Junping Zhang[1], Juntao Zhou[2], Yanna Liu[1], Ning Xu[3,*]

[1]Department of Anesthesiology, Shenzhen Longhua District Central Hospital, 518110 Shenzhen, Guangdong, China
[2]Colorectal Surgery, Shenzhen Longhua District Central Hospital, 518110 Shenzhen, Guangdong, China
[3]Department of Medical Imaging, Shenzhen Longhua District Central Hospital, 518110 Shenzhen, Guangdong, China
*Correspondence: zhixinghuoda@163.com (Ning Xu)
Published: 20 July 2024

Background: Melanoma is a highly invasive skin cancer with limited treatment strategies. Bupivacaine, a commonly used local anesthetic recognized for its safety, has shown promise in combating tumors. 3′-phosphoadenosine 5′-phosphosulfate synthase 2 (PAPSS2) is a key enzyme in the sulfation process and is associated with the development and metastasis of various tumors. This study aimed to explore the mechanism by which bupivacaine inhibits melanoma proliferation and metastasis by targeting PAPSS2.

Methods: The effects of bupivacaine on the proliferation of A375 and A2058 melanoma cells were evaluated using Cell Counting Kit-8 (CCK-8), 5-Ethynyl-2'-deoxyuridine (EdU) labeling, and clonogenic assays. Cell migration, invasion, and PAPSS2 expression were evaluated using Transwell experiments and Quantitative Reverse Transcription Polymerase Chain Reaction (qRT-PCR) analysis. Additionally, an *in vivo* melanoma tumor model in nude mice was constructed to evaluate the impact of bupivacaine on melanoma growth and metastasis. Immunohistochemistry was used to assess tumor metastasis and PAPSS2 expression levels in the nude mouse model.

Results: Experimental results demonstrated that bupivacaine significantly inhibited melanoma proliferation and invasion compared to the control group. Notably, this inhibitory effect was partially reversed by PAPSS2 overexpression. *In vivo* experiments demonstrated that bupivacaine-treated nude mice exhibited reduced tumor volumes, weights, and fewer lung metastatic foci. Molecular analysis via qRT-PCR and immunohistochemistry analysis further indicated that bupivacaine significantly reduced PAPSS2 in tumor tissues.

Conclusion: This study confirms that bupivacaine, a local anesthetic, can inhibit melanoma proliferation and metastasis by targeting the PAPSS2 signaling pathway. These findings suggest its potential as an anti-tumor medication and present new treatment strategies for melanoma.

Keywords: bupivacaine; melanoma; PAPSS2; proliferation; metastasis

Introduction

Melanoma is a malignant tumor originating from pigment cells, characterized by its high invasiveness, rapid progression, and challenging late-stage treatment [1,2]. According to the World Health Organization (WHO), approximately 132,000 new cases of melanoma are diagnosed each year, and the incidence continues to rise [3–5]. Although melanoma does not have the highest incidence among malignant skin tumors, its mortality rate far exceeds that of other skin cancer types [6]. Therefore, the development of new treatment strategies, particularly those targeting tumor proliferation and metastasis, is of great significance for improving the survival rate of melanoma patients [7,8]. In recent years, targeted therapy and immunotherapy have emerged as new directions in melanoma treatment [9–11]. However, the high heterogeneity of melanoma and the challenge of post-treatment drug resistance limit the effectiveness of these approaches to only a subset of patients, with long-term efficacy remaining inadequate [12,13]. Therefore, exploring new treatment targets and drugs, especially those that can affect the tumor microenvironment and the biological characteristics of tumor cells, has become a focal point of research [14].

3′-phosphoadenosine 5′-phosphosulfate synthase 2 (PAPSS2) is an enzyme expressed in various tissues, primarily responsible for catalyzing the generation of 3′-phosphoadenosine 5′-phosphosulfate (PAPS), the main donor in sulfation reactions involved in the sulfation modification of various biological molecules [15,16]. These sulfation modifications are crucial for biological processes such as protein function, cell signaling, and extracellular matrix construction [17]. Recent studies have found that the expression of PAPSS2 is associated with the malignancy of certain cancers, suggesting its potential significance in tumor development [17–19].

Bupivacaine is a commonly used local anesthetic that primarily functions by blocking sodium channels on neuronal membranes, thereby inhibiting the conduction of nerve impulses [20–22]. In addition to its anesthetic effect, mounting evidence indicates that local anesthetics (including bupivacaine) also have anti-inflammatory and antitumor potential [20,23]. Several *in vitro* and *in vivo* studies have demonstrated that bupivacaine can inhibit the proliferation of various types of cancer cells and influence the tumor microenvironment [24,25]. However, the molecular mechanism of bupivacaine in its anti-melanoma effects remains unclear.

This study aims to explore the impact of bupivacaine on the proliferation and metastasis of melanoma cells, along with its potential molecular mechanism. Our focus centers on assessing whether bupivacaine can exert its anti-tumor effects by targeting PAPSS2. Using both cell and animal models, we expect to reveal the influence of bupivacaine on PAPSS2 and its implications on melanoma proliferation and metastasis. This research may provide new targets for the treatment of melanoma and lay a theoretical foundation for clinical applications.

Materials and Methods

Cell Culture

Melanoma cell lines A375 (CL-0014) and A2058 (CL-0652) were obtained from Procell (Wuhan, China). Fetal Bovine Serum (FBS) (iCell-0500) and Dulbecco's Modified Eagle Medium (DMEM) (iCell-138-0001) culture media were purchased from iCell (Shanghai, China). Cell cultures were maintained at 37 °C in a 5% CO_2 humidified incubator using high-glucose DMEM medium supplemented with 10% fetal bovine serum and 1% penicillin-streptomycin. The culture medium was changed every 3 days, and cells were collected using 0.25% trypsin for digestion. Cells in the logarithmic growth phase were selected for experimentation. Cell identification was confirmed by STR analysis and mycoplasma detection.

Cell Transfection

A fusion expression vector containing the full-length *PAPSS2* gene and its functional domain deletion mutant was constructed. Lentivirus vector-mediated *PAPSS2* shRNA (Open Biosystems) was used, with the following sequences utilized: *PAPSS2* shRNA-1: TTTGGCTTTGTTGTAGGCAGC and *PAPSS2* shRNA-2: AATCCGAGATTTCTGTTAAGG. The overexpression (OE) *PAPSS2* sequence consisted of 5′-TAAGCTTATGTCGGGGATCAA-3′ (forward) and 5′-TGTCGACTTAGTTCTTCTCCA-3′ (reverse). Empty vector and *PAPSS2* gene were transfected into cells according to the manufacturer's instructions for the transfection reagent. Stable transfected and expressing cells were selected using G418 (800 μg/mL) (VT024457, Solarbio, Beijing, China). Stable transduced cells were selected using puromycin (5 μg/mL) (P8230, Solarbio, Beijing, China), and clones were expanded and cultured. Western blotting was used for validation.

Cell Counting Kit-8 (CCK-8) Assay

Cells were seeded into 96-well plates at a density of approximately 3500 cells per well and cultured at 37 °C in a 5% CO_2-humidified atmosphere. Subsequently, 10 μL of CCK-8 reagent was added to each well, followed by incubation for an additional 2 hours in the cell culture incubator (Heracell™ VIOS Series, Thermo Fisher Scientific, Waltham, MA, USA). Absorbance (A) at a wavelength of 450 nm was measured using a microplate reader (Multiskan™ FC, Thermo Fisher Scientific, Waltham, MA, USA) to calculate the cell proliferation rate. The experiment was repeated three times.

5-Ethynyl-2'-deoxyuridine (EdU) Experiment

Cells were cultured in a medium containing 50 μmol/L EdU for 2 hours, following the instructions outlined in the EdU detection kit (CA1170, Solarbio, Beijing, China). Subsequently, cells were stained, and images were acquired using an inverted fluorescence microscope (IX83, Olympus, Tokyo, Japan) in five distinct fields: upper left, lower left, upper right, lower right, and center (magnification ×200). The number of EdU-positive cells (in red) was quantified to calculate the cell proliferation rate, expressed as the percentage of EdU-positive cells relative to the total cell number. The experiment was repeated three times.

Clonogenic Assay

Cells were seeded into 6-well plates at a density of approximately 500 cells per well. Following a 7-day incubation period, the supernatant was removed, and the cells were fixed with 4% paraformaldehyde (P1110, Solarbio, Beijing, China) for 20 minutes. Subsequently, staining with 0.1% crystal violet (G1062, Solarbio, Beijing, China) was performed for 15 minutes, after which the plates were observed under the microscope (CX53, Olympus, Tokyo, Japan) to determine the number of formed colonies and calculate the clonogenic rate.

Transwell Assay

Transwell chambers were placed in a 24-well plate, with 600 μL of medium containing 20% fetal bovine serum added to the lower chamber. Cells in the logarithmic growth phase were suspended in a serum-free medium and adjusted to a density of 3×10^5 cells/mL. The cell suspension was then added to the upper chamber. After culturing for 36 hours, cells in the upper chamber were removed using a cotton swab. The cells at the bottom of the chamber were fixed with 40 g/L paraformaldehyde for 15 minutes and subsequently stained with crystal violet solution for 15 minutes. Images were captured using an inverted microscope (IX83, Olympus, Tokyo, Japan), and cell counting was performed

in five fields (×400), with the average counts from the five fields used for analysis. The experiment was repeated three times.

Quantitative Reverse Transcription Polymerase Chain Reaction (qRT-PCR)

Total RNA was extracted from cells according to the Trizol (15596026, Invitrogen, Carlsbad, CA, USA) manual. 2 µg of RNA was used to synthesize cDNA according to the reverse transcription kit instructions. For qRT-PCR analysis, 0.5 µL of diluted cDNA was used and the relative expression levels were detected using SYBR Green fluorescent dye (S7574, Invitrogen, Carlsbad, CA, USA). Glyceraldehyde 3-phosphate dehydrogenase (*GAPDH*) was used as the internal reference gene. The primer sequences for *PAPSS2* were as follows: forward primer, 5′- GACCAGCAAAAATCCACCAATG -3′; reverse primer, 5′- CACACGGTACATCCTCGGAAT -3′. The *GAPDH* primers were as follows: forward 5′- AGGTCGGTGTGAACGGATTTG -3′, reverse 5′- GGGGTCGTTGATGGCAACA -3′. The primer sequences for Matrix Metalloproteinase-9 (*MMP-9*) were as follows: forward primer 5′- GCAGAGGCATACTTGTACCG -3′, reverse primer 5′- TGATGTTATGATGGTCCCACTTG -3′. The primer sequences for *MMP-1* were as follows: forward primer 5′- AAAATTACACGCCAGATTTGCC -3′, reverse primer 5′- GGTGTGACATTACTCCAGAGTTG -3′. The primer sequences for *MMP-2* were as follows: forward primer 5′- ACCTGAACACTTTCTATGGCTG -3′, reverse primer 5′- CTTCCGCATGGTCTCGATG -3′.

Fluorescence intensity was measured using a qRT-PCR instrument (QuantStudio 7, Thermo Fisher Scientific, Waltham, MA, USA) with the following cycling conditions: 95 °C for 5 minutes for one cycle, followed by 40 cycles of denaturation at 95 °C for 15 seconds, annealing at 60 °C for 60 seconds, and extension at 72 °C for 30 seconds. Each sample was set up in triplicate, and the $2^{-\Delta\Delta CT}$ method was used to calculate relative expression levels.

Western Blot

After transfecting A375 cells for 48 hours, cells were digested with 0.25% trypsin and placed in a 1.5 mL centrifuge tube. The cells underwent a single wash with cold PBS and were subsequently resuspended in 200 µL of 1× SDS buffer and boiled at 95 °C for 10 minutes. The supernatant was obtained after centrifugation at 1000 r/min for 10 minutes and was collected as total protein. The samples were loaded onto SDS-PAGE gel wells according to standard procedures. Semi-dry transfer was used to transfer the proteins to a PVDF membrane (88518, Invitrogen, Carlsbad, CA, USA), followed by blocking with 5% skimmed milk at room temperature for 1 hour. After washing with Tris-Buffered Saline with Tween (TBST), primary antibodies were added for PAPSS2 (ab155585, Abcam, Cambridge, UK, 1:400), MMP-2 (ab92536, 1:400, Abcam, Cambridge, UK), MMP-9 (ab76003, 1:400, Abcam, Cambridge, UK), and β-actin (ab7817, Abcam, Cambridge, UK) at a dilution of 1:1000. Incubation was conducted at 4 °C for 24 hours, followed by further washing with TBST and the addition of secondary antibodies (1:5000). After incubation at room temperature for 1 hour and subsequent washing with TBST, ECL luminescence solution was added to enhance visualization. Protein bands were then analyzed using a gel imaging system and Image J software (version 1.5f, NIH, Bethesda, MD, USA) for grayscale intensity.

Immunofluorescence Staining

After 2–3 generations of culture, cells were washed with PBS and fixed with 4% paraformaldehyde for 10 minutes. After three PBS washes, rabbit anti-mouse primary antibody for PAPSS2 (Abcam, Cambridge, UK, ab155585, 1:500) was added and incubated overnight at 4 °C in a humidified chamber. Following another three PBS washes, goat anti-rabbit FITC or PE fluorescent secondary antibody (Abcam, Cambridge, UK, ab6714, ab6718, 1:1000) was added. After additional PBS washing, DAPI was used for nuclear counterstaining, followed by a 5-minute incubation at room temperature in the dark. The observation was conducted using a fluorescence confocal microscope.

Bioinformatics Analysis

The expression of PAPSS2 in both melanoma tumor tissues and adjacent normal tissues was analyzed using data from the Human Protein Atlas (HPA) database. The immunohistochemical staining images of PAPSS2 in both tumor and healthy tissues were also downloaded from the HPA database. The Human Protein Atlas (HPA) database (https://www.proteinatlas.org/) was utilized to detect the protein expression of PAPSS2 and its correlation with the prognosis of melanoma patients. The HPA database aims to integrate various omics technologies to explore the human proteome, serving as a public database. Specifically, the "PATHOLOGY" module was used to examine the relationship between the PAPSS2 expression levels in melanoma patients and their prognosis.

Subcutaneous Xenograft Model

SPF-grade female nude mice, aged 6–8 weeks old and weighing 18–20 g, were purchased from Beijing Sibeifu Biotechnology Co., Ltd. (Beijing, China), with animal license number SCXK (Beijing) 2021-0105. This study was approved by the Committee of Shenzhen Longhua District Central Hospital (No.2021-163-01). A375 cells were cultured *in vitro*, and cells in the logarithmic growth phase were used to adjust the cell concentration to 2.5×10^6/mL using 1× PBS. Subsequently, subcutaneous inoculation of 0.2 mL/mouse was performed in the right forelimb axilla of the nude mice. Evaluation of melanoma growth inhibition was conducted by measuring the length and width of the

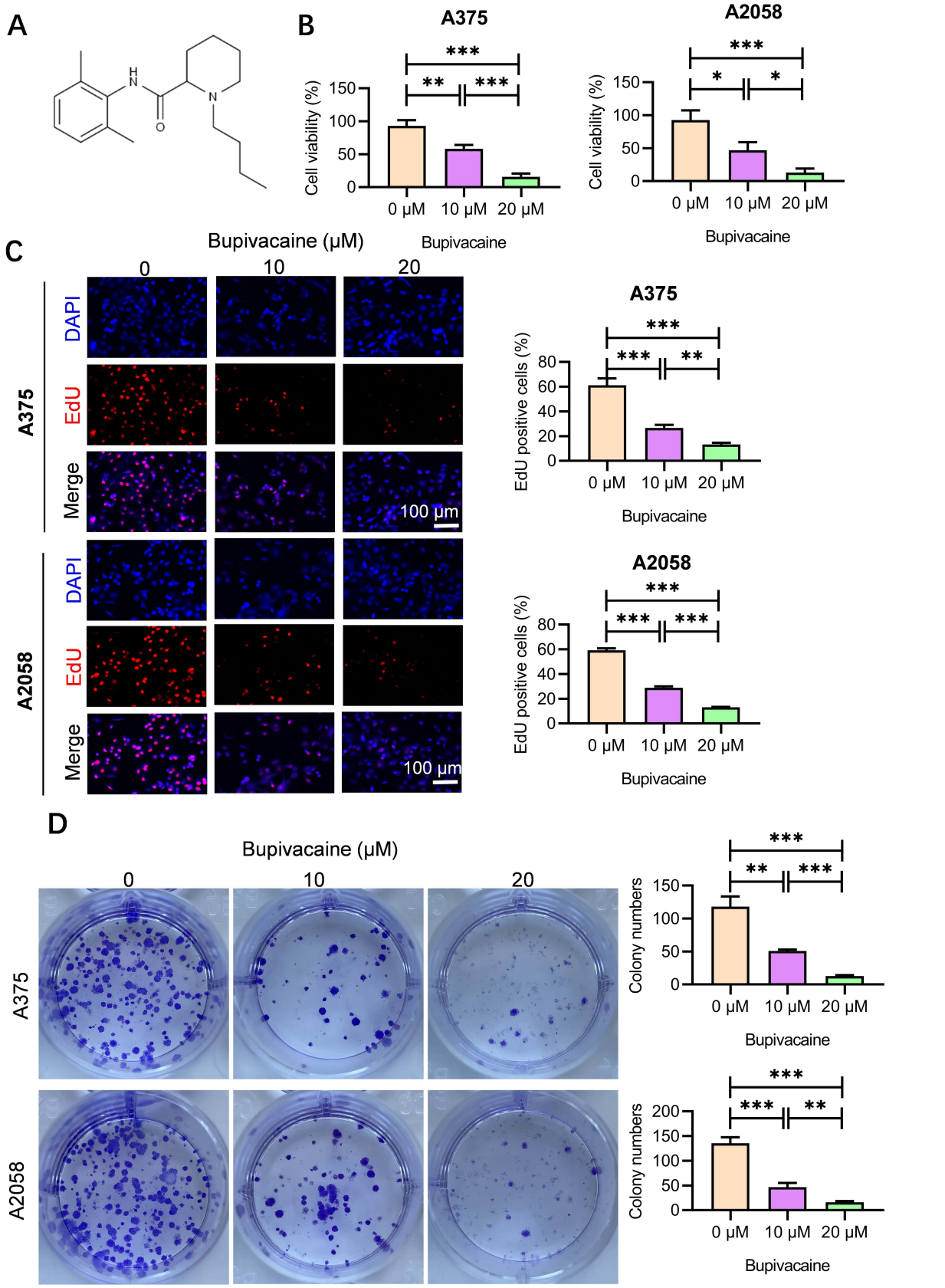

Fig. 1. Inhibition of melanoma cell proliferation by bupivacaine. (A) Chemical structure of bupivacaine. (B) A375 and A2058 cells were separately seeded in 96-well plates and treated with bupivacaine for 24 hours, followed by a Cell Counting Kit-8 (CCK-8) assay to detect cell proliferation. (C) 5-Ethynyl-2'-deoxyuridine (EdU) assay to measure cell proliferation. Scale bar = 100 μm. (D) Clonogenic assay to assess cell proliferation. *$p < 0.05$, **$p < 0.01$, ***$p < 0.001$. n = 3.

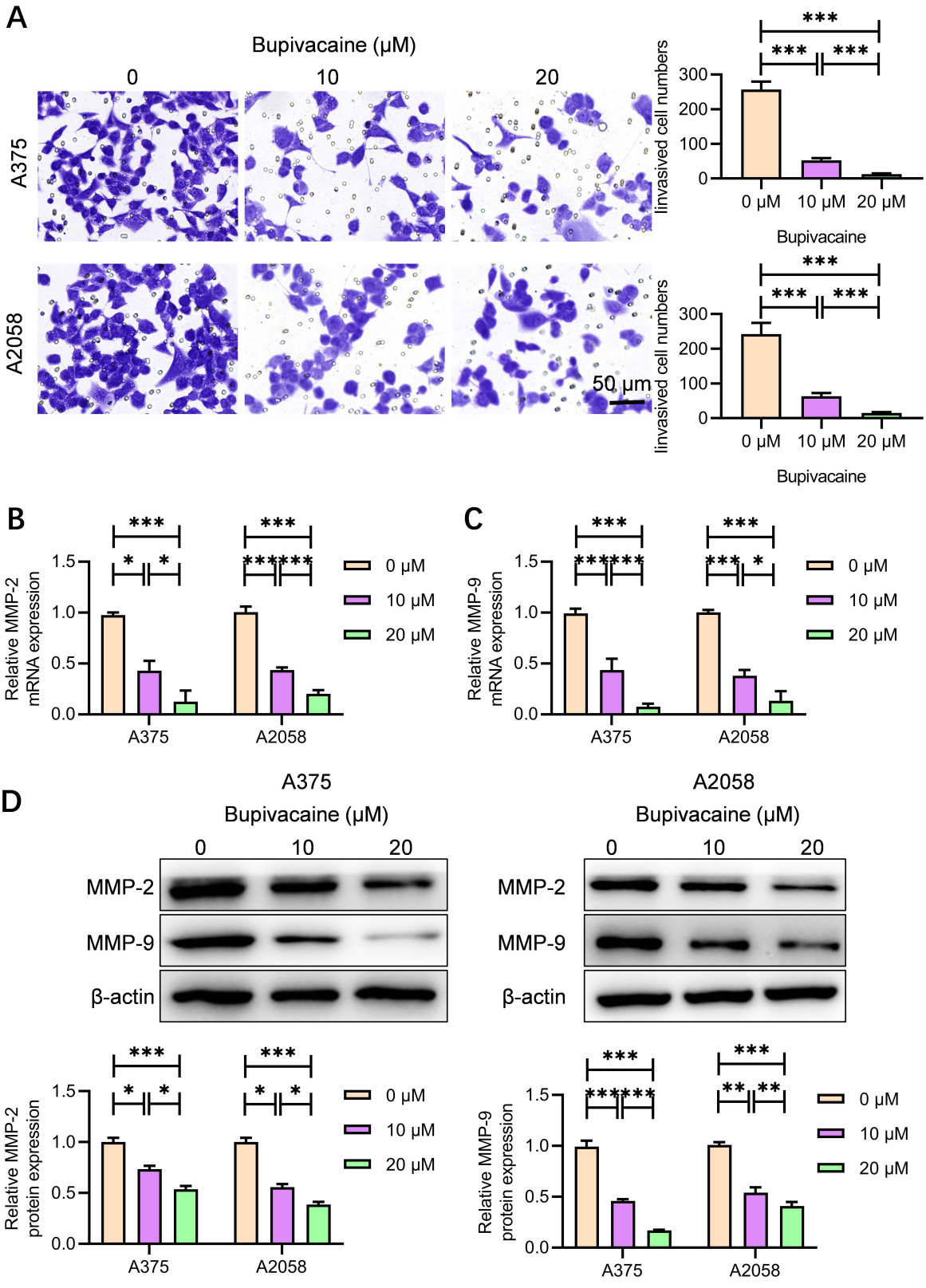

Fig. 2. Inhibition of melanoma cell migration by bupivacaine. (A) Cells were treated with different concentrations of bupivacaine (0, 10, and 20 μM) and subjected to Transwell assay to measure cell migration. Scale bar = 50 μm. (B,C) qRT-PCR analysis identified changes in Matrix Metalloproteinase-2 (MMP-2) (B) and MMP-9 (C) expression. (D) Western blot analysis of MMP-2 and MMP-9 expression levels. qRT-PCR, Quantitative Reverse Transcription Polymerase Chain Reaction. *$p < 0.05$, **$p < 0.01$, ***$p < 0.001$. n = 3.

tumor mass using a caliper when the subcutaneous tumor mass was palpable (i.e., assessing the longest and shortest diameters). Tumor volume was calculated using length × width × width, and a tumor growth curve was plotted accordingly. Intraperitoneal drug administration commenced seven days after subcutaneous inoculation of melanoma and continued for 14 consecutive days. Following this treatment period, euthanize nude mice via intraperitoneal injection of pentobarbital sodium (3 mg/mL) (110 mg/kg). The tumor mass was removed and weighed, and the tumor inhibition rate was calculated as (1 – tumor mass of each treatment group/tumor mass of the model group) × 100%. Finally, the tumor tissue was wrapped in aluminum foil and stored at –80 °C for future use.

Hematoxylin and Eosin (HE) Staining

After dehydration and embedding of lung tissue, it was sectioned into 4-µm sections, affixed to glass slides, and incubated in a 42 °C oven overnight. The sections were then placed in an oven and baked at 60 °C for 1 hour. Deparaffinization and rehydration were performed using an alcohol gradient. After deparaffinization, the sections were soaked in distilled water and gently shaken for 4 minutes on a shaker bed to remove residual alcohol. Cell nuclei were stained with hematoxylin solution for 2 minutes and subsequently rinsed with running water for 6 minutes. Following differentiation with 1% hydrochloric acid alcohol, Hematoxylin and Eosin staining was performed for 3 minutes, followed by rinsing with running water for 6 minutes. The sections were dehydrated and sealed by sequentially placing them in 70%, 80%, and 95% ethanol solutions, absolute ethanol, a 1:1 mixture of ethanol and xylene, and xylene. Sections were then air-dried and sealed with neutral gum. Microscopic (IX83, Olympus, Tokyo, Japan) observation and photography were then conducted.

Immunohistochemical Staining

The deparaffinization of paraffin sections replicated the process used for HE staining. Antigen retrieval was performed by immersing the sections in citric acid retrieval solution and heating them in a microwave on high for 5 minutes. The repaired tissue sections were promptly transferred to preheated distilled water, allowed to cool to room temperature, shaken for 4 minutes, and then washed twice with PBS buffer. Subsequently, 3% H_2O_2 was applied to the sections, and the reaction was conducted in a dark box to eliminate endogenous peroxidase. Membrane permeabilization was achieved by adding 0.1% Triton X-100, followed by incubation at room temperature for 10 minutes, and three washes with PBS. Goat serum blocking was carried out by incubating the sections with goat serum at room temperature for 1 hour, followed by five washes with PBS buffer. Next, the sections were incubated overnight at 4 °C in a humid chamber with the primary antibody for PAPSS2 (1:100 dilution). Subsequently, the sections were incubated with the secondary antibody (1:200 dilution) in the dark at room temperature for 60 minutes. DAB color development was then performed, followed by observation and photography using a microscope (IX83, Olympus, Tokyo, Japan). Lastly, the immunohistochemical staining intensity was quantified.

Statistical Analysis

SPSS statistical software (version 19.0, IBM, Armonk, NY, USA) was used for statistical analysis. Continuous data were normally distributed and presented as mean ± standard deviation. Between-group comparisons were performed using *t*-tests while multi-group comparisons were conducted via one-way analysis of variance (ANOVA). Statistical significance was considered at $p < 0.05$.

Results

Bupivacaine Inhibits the Proliferation of Melanoma Cells

Based on the findings depicted in Fig. 1, it was observed that the proliferation ability of A375 and A2058 cells decreased in a dose-dependent manner under treatment with varying concentrations of bupivacaine. Both the CCK-8 and EdU assays revealed a significant decrease in cell proliferation with increasing bupivacaine concentrations (Fig. 1A–C). The clonogenic assay results demonstrate a pronounced inhibitory effect of bupivacaine on melanoma cell proliferation, which is enhanced with increasing bupivacaine concentration (Fig. 1D, $p < 0.05$).

Bupivacaine Inhibits Melanoma Cell Migration

Transwell experiments demonstrated a dose-dependent decrease in melanoma cell migration with increasing bupivacaine concentration (Fig. 2A, $p < 0.001$). qRT-PCR analysis revealed decreasing MMP-2 and MMP-9 levels with increasing bupivacaine concentration (Fig. 2B,C, $p < 0.05$ and $p < 0.001$). Moreover, Western blot analysis confirmed this trend, indicating a dose-dependent decrease in MMP-2 and MMP-9 protein expression levels with increasing bupivacaine concentration (Fig. 2D, $p < 0.05$ and $p < 0.001$). These results suggest that bupivacaine treatment significantly inhibits the migration ability of melanoma cells by downregulating MMP-2 and MMP-9.

Bupivacaine Inhibits PAPSS2 Expression and Activation

qRT-PCR analysis was used to evaluate the *PAPSS2* mRNA expression levels in melanoma cells A375 and A2058 following bupivacaine treatment. The results show a dose-dependent decrease in *PAPSS2* mRNA expression as bupivacaine concentration increased (Fig. 3A), indicating that bupivacaine can inhibit the transcriptional activity of the *PAPSS2* gene. After 24 hours of treatment with dif-

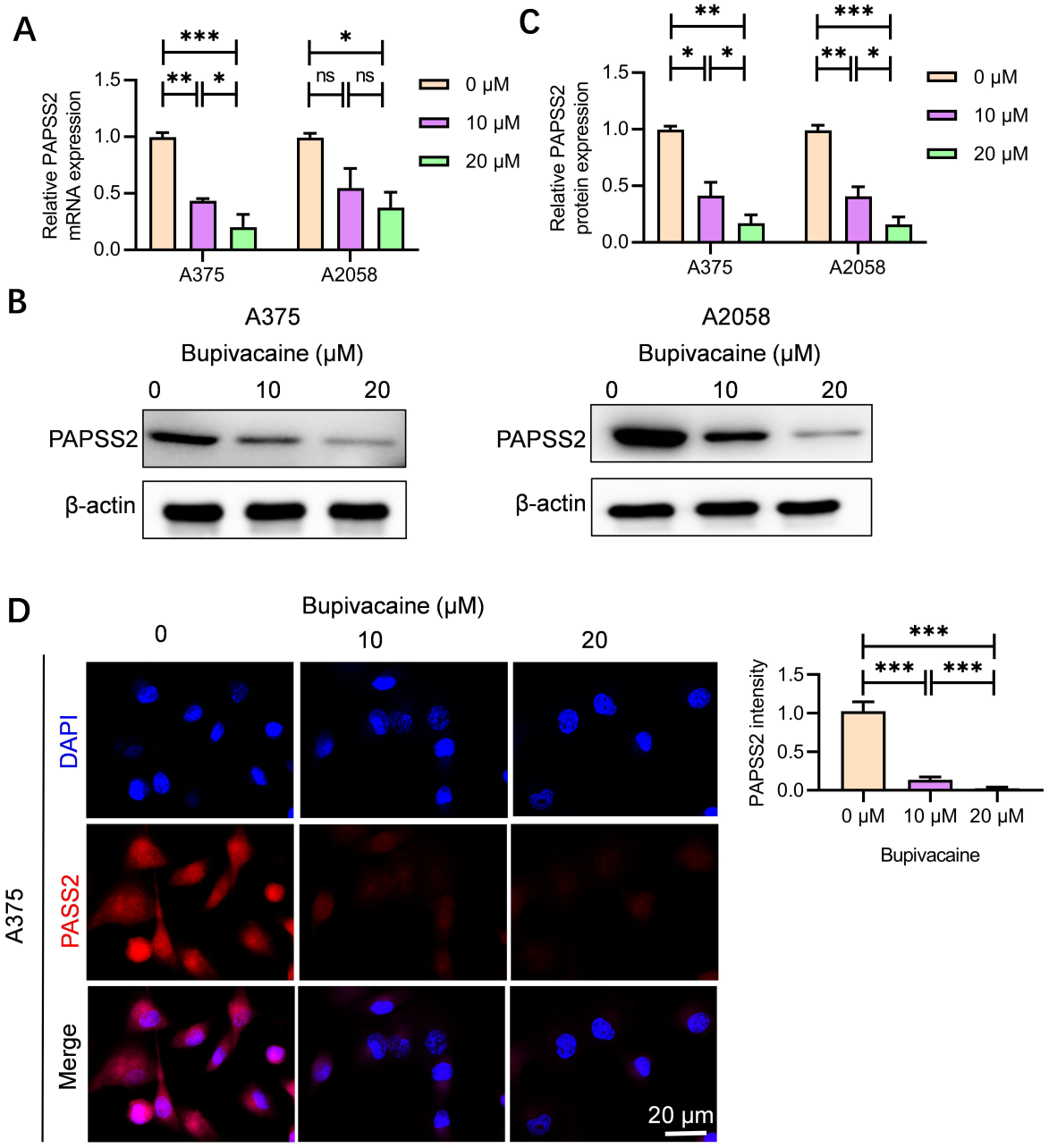

Fig. 3. Inhibition of 3′-phosphoadenosine 5′-phosphosulfate synthase 2 (PAPSS2) expression and activation by bupivacaine. (A–C) Quantitative qRT-PCR analysis (A) and Western blot (B,C) of PAPSS2 in A375 and A2058 cells treated with different concentrations of bupivacaine (0, 10, and 20 μM) for 24 hours. (D) Immunofluorescence staining of PAPSS2 in A375 cells treated with different concentrations of bupivacaine (0, 10, and 20 μM) for 24 hours. Scale bar = 20 μm. *p <0.05, **p < 0.01, ***p <0.001. ns, not statistically significant.

ferent concentrations of bupivacaine, the protein expression levels of *PAPSS2* in A375 and A2058 cells also decreased, aligning with the decreasing mRNA levels (Fig. 3B,C). This finding further corroborates the effect of bupivacaine in reducing PAPSS2 protein expression. Immunofluorescence staining was used to detect and localize specific proteins within cells. In A375 cells, the fluorescence intensity of PAPSS2 decreased with increasing bupivacaine concentration, consistent with the results of qRT-PCR and Western blot. This observation further substantiates the ability of bupivacaine to inhibit cellular PAPSS2 expression (Fig. 3D).

PAPSS2 is Highly Expressed in Melanoma and is Negatively Correlated with Prognosis

The results in Fig. 4A,B demonstrate that the expression of PAPSS2 in melanoma tissues is higher than in adjacent normal tissues (tumor > adjacent normal). This ob-

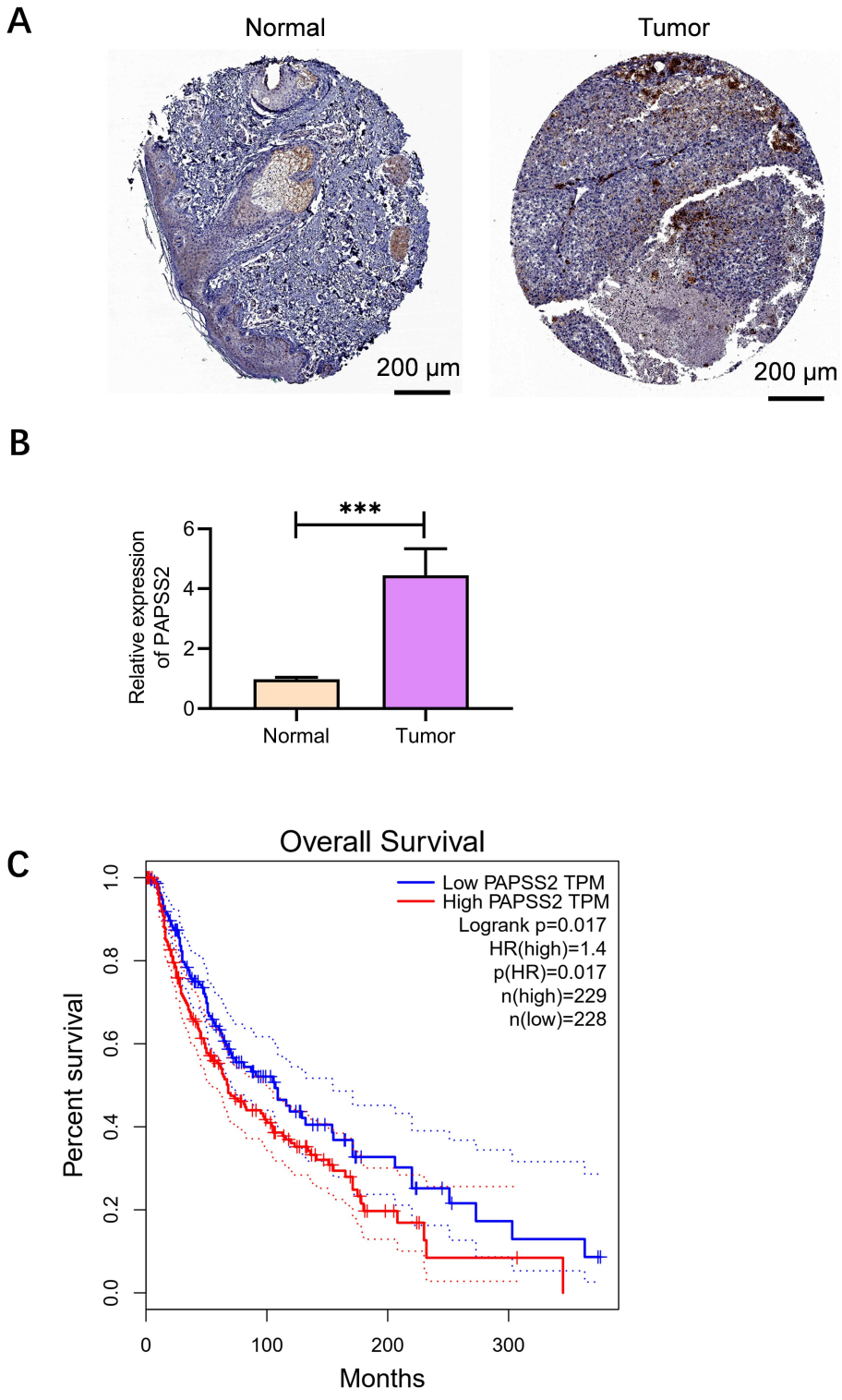

Fig. 4. High expression of PAPSS2 in melanoma and its negative correlation with prognosis. (A) High expression of PAPSS2 in melanoma. (B) The statistical plot of PAPSS2 in melanoma. (C) Poor prognosis in patients with high PAPSS2 expression. ***$p < 0.001$. n = 3.

servation suggests that PAPSS2 may promote the development of melanoma, possibly by promoting tumor proliferation and metastasis through its influence on the sulfation reaction in tumor cells. In addition, survival analysis results demonstrate that melanoma patients with high levels of PAPSS2 expression have a poorer prognosis (Fig. 4C). This may be due to the promotion of tumor proliferation and metastasis by elevated PAPSS2 expression levels, in-

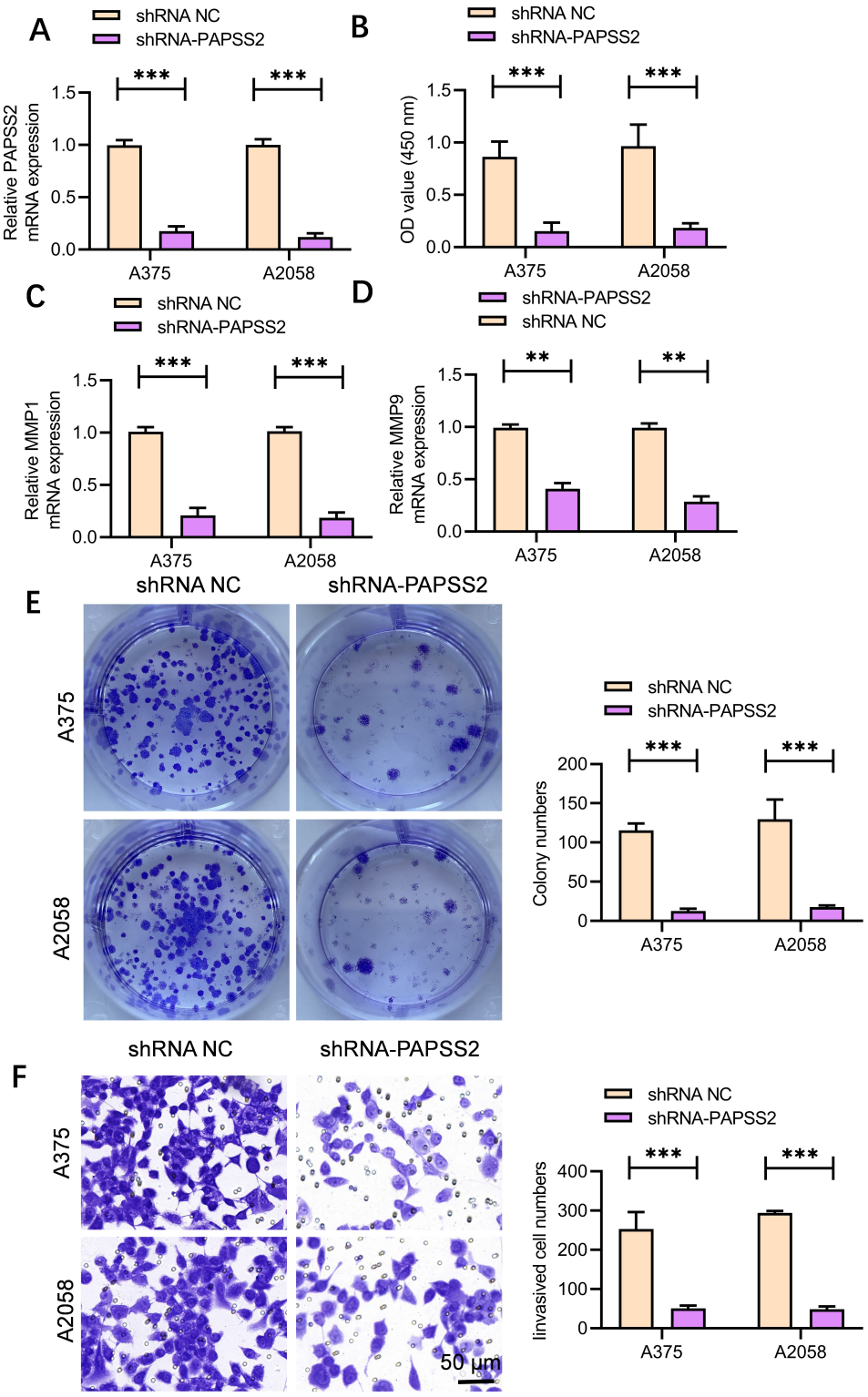

Fig. 5. Downregulation of PAPSS2 expression inhibits melanoma progression. (A) Knockdown efficiency of shRNA targeting PAPSS2 in A375 and A2058 cells. (B) Analysis of cell proliferation following transfection with shRNA-NC or shRNA-PAPSS2 in A375 and A2058 cells. (C) Expression level of MMP-1 with shRNA-NC or shRNA-PAPSS2 in A375 and A2058 cells. (D) Expression level of MMP-9 with shRNA-NC or shRNA-PAPSS2 in A375 and A2058 cells. (E) Clonogenic assay. (F) Transwell invasion assay. Scale bar = 50 μm. $^{**}p < 0.01$, $^{***}p < 0.001$. n = 3.

creasing difficulty in treatment and control. PAPSS2 may play an important role in the development of melanoma and its expression level is closely associated with patient prognosis.

Inhibition of the PAPSS2 Signaling Pathway Suppresses Melanoma Cell Proliferation and Migration

qRT-PCR was used to assess the transfection efficiency of shRNA-PAPSS2, revealing that the expression of PAPSS2 in the shRNA-PAPSS2 group was notably lower than in the shRNA-NC group, suggesting successful inhibition of PAPSS2 expression by shRNA (Fig. 5A). The proliferation ability of A375 and A2058 cells transfected with shRNA-PAPSS2 was lower than that of the control group, indicating that inhibition of PAPSS2 can suppress melanoma cell proliferation (Fig. 5B). Considering bupivacaine may directly affect the expression of these proteins, we tested the expression of MMP-1 and MMP-9, finding reduced expression in the shRNA-PAPSS2 group compared to the shRNA-NC group (Fig. 5C,D). Clonogenic assays were performed to evaluate the growth and proliferation ability of cells. The clonogenic assays revealed a reduction in the number of colonies formed by cells transfected with shRNA-PAPSS2 compared to the control group, further confirming that inhibition of PAPSS2 can reduce melanoma cell proliferation (Fig. 5E). Additionally, Transwell invasion assays were conducted to assess the invasion ability of cells. The results indicate that cells transfected with shRNA-PAPSS2 exhibit reduced invasion ability compared to the control group, suggesting that PAPSS2 inhibition reduces the invasiveness of melanoma cells (Fig. 5F).

Overexpression of PAPSS2 Reverses the Antitumor Effect of Bupivacaine

The *PAPSS2* mRNA expression level was detected by qRT-PCR to verify the transfection efficiency of the overexpression vector, indicating higher levels in the OE-PAPSS2 group compared to the OE-NC group, suggesting successful PAPSS2 overexpression (Fig. 6A). Cellular proliferation ability was evaluated to observe the effect of bupivacaine on melanoma cells, identifying reduced levels in the bupivacaine-treated group compared to the control group. However, in the case of PAPSS2 overexpression (bupivacaine+OE-PAPSS2), cellular proliferation ability was higher than that of the bupivacaine group, indicating that PAPSS2 overexpression can reverse the antitumor effects of bupivacaine (Fig. 6B). Meanwhile, results show higher MMP-1 and MMP-9 expression levels in the OE-PAPSS2 group compared to the OE-NC group, indicating successful PAPSS2 overexpression (Fig. 6C,D). Changes in cell invasion ability were further investigated through Transwell experiments to explore bupivacaine's underlying mechanism of action. The experimental results show that the migration ability of the bupivacaine-treated group was reduced, whereas the migration ability of the group overexpressing PAPSS2 was restored. These findings indicate that PAPSS2 may be a key factor in bupivacaine's effect on melanoma cell migration (Fig. 6E).

Bupivacaine Suppresses Tumor Growth and Metastasis in Melanoma by Inhibiting the PAPSS2 Signaling Pathway

Results from the subcutaneous xenograft animal experiment show that the tumor volume of the control group was significantly larger than that of the bupivacaine-treated group, suggesting that bupivacaine has an inhibitory effect on melanoma tumor growth (Fig. 7A). The growth curve can reflect the dynamic progression of tumor growth and serves as an important parameter for evaluating drug effects. Accordingly, the tumor growth rate and volume of the bupivacaine-treated group were lower than those of the control group, further confirming bupivacaine's inhibitory effect (Fig. 7B, $p < 0.01$). Tumor weight is a direct and objective indicator for evaluating tumor growth. The tumor weight of the bupivacaine-treated group was significantly lower than that of the control group, aligning with the observation of tumor volume and further validating the inhibitory effect of bupivacaine on tumor growth (Fig. 7C, $p < 0.001$). The presence of tumor cells in the lungs was observed via HE staining. The number of pulmonary metastatic lesions in the control group was greater than in the bupivacaine-treated group, indicating that bupivacaine may inhibit melanoma metastasis (Fig. 7D,E, $p < 0.01$). The expression level of PAPSS2 in tumor tissues was detected by qRT-PCR and immunohistochemistry, demonstrating reduced levels in the bupivacaine-treated group compared to the control group. These findings suggest that bupivacaine may exert its inhibitory effect on tumors by downregulating PAPSS2 expression (Fig. 7F,G, $p < 0.05$ and $p < 0.001$).

Discussion

This study identified a novel finding, demonstrating that the local anesthetic bupivacaine inhibits the proliferation and metastasis of melanoma by targeting PAPSS2. The results of this study indicate that bupivacaine not only significantly inhibits the *in vitro* proliferation of melanoma cell lines but also reduces their metastatic capability in a nude mouse model. These findings provide new insights into the potential anti-tumor activity of local anesthetics, specifically through PAPSS2 downregulation.

PAPSS2 is a key enzyme in the sulfation pathway, facilitating the synthesis of 3′-phosphoadenosine 5′-phosphosulfate (PAPS), a common substrate utilized by sulfotransferases for sulfation modification of various biological molecules [15,18]. Sulfation plays an important role in regulating the extracellular matrix composition, cell signaling, cell adhesion, and tumor metastasis [26,27]. Previous

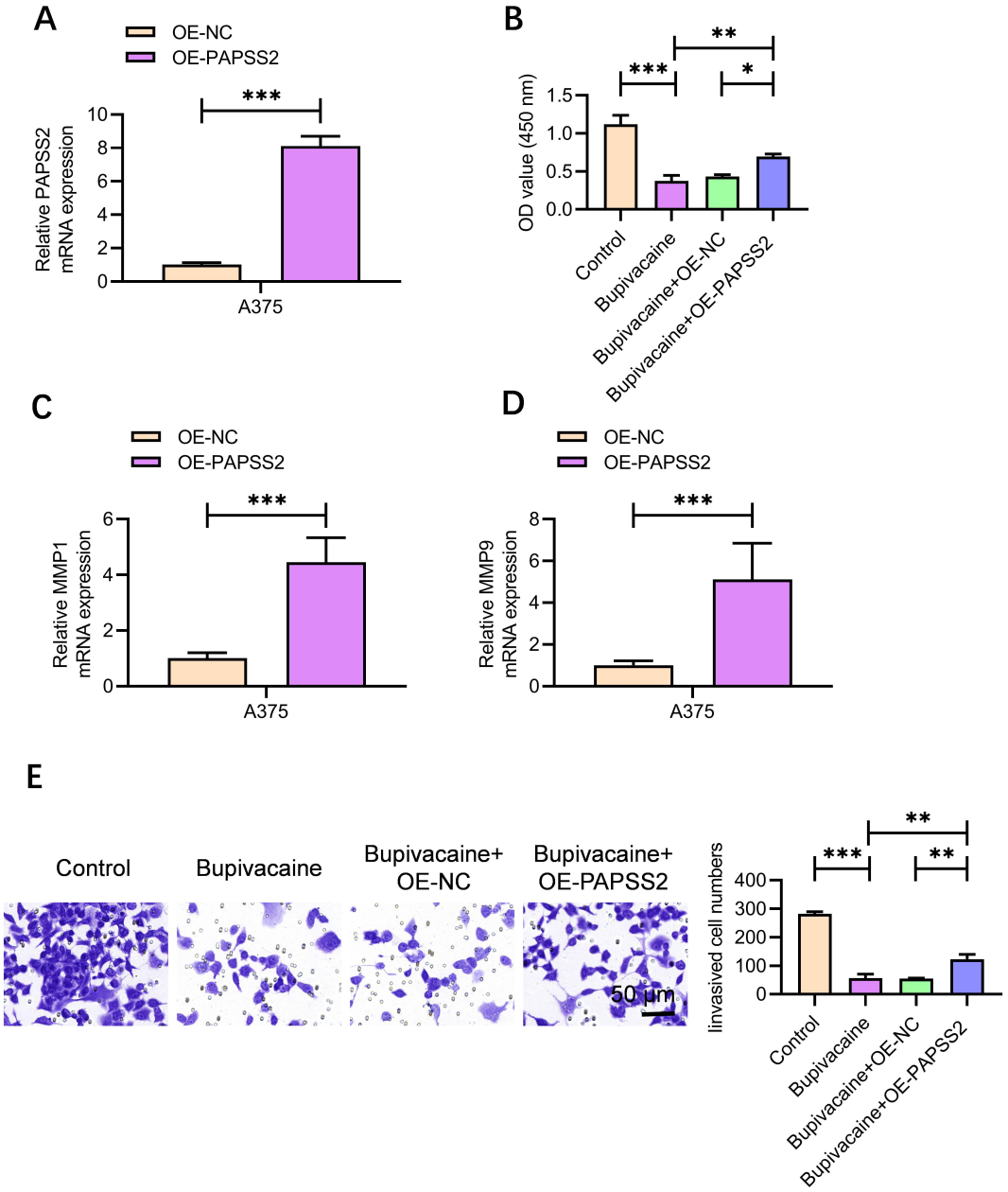

Fig. 6. Overexpression of *PAPSS2* reverses the anti-tumor effect of bupivacaine. (A) Overexpression efficiency of *PAPSS2* in A375. (B) Analysis of cell proliferation following overexpression of PAPSS2 in A375. (C) Expression level of *MMP-1* following overexpression of *PAPSS2* in A375 cells. (D) Expression level of *MMP-9* following overexpression of *PAPSS2* in A375 cells. (E) Transwell invasion assay following overexpression of *PAPSS2* in A375 and A2058 cells. Scale bar = 50 μm. *$p < 0.05$, **$p < 0.01$, ***$p < 0.001$. n = 3.

studies have indicated that PAPSS2 is upregulated in certain cancers and is associated with malignancy [18,19]. However, little is known about the role of PAPSS2 in melanoma and its potential as a drug target.

This study revealed a significant decrease in the proliferation and invasive capacity of melanoma cells following transfection with shRNA-PAPSS2, suggesting the pivotal role of PAPSS2 in melanoma cell proliferation and invasion. Additionally, PAPSS2 overexpression reversed the inhibitory effect of bupivacaine on melanoma cell proliferation and invasion, indicating that bupivacaine exerts its anti-tumor effect by inhibiting PAPSS2. In a nude mouse tumor model, treatment with bupivacaine led to notable reductions in tumor growth rate, tumor weight, and lung metastases. These results further validate the inhibition of melanoma proliferation and metastasis by bupivacaine through PAPSS2 inhibition. qRT-PCR and immunohistochemical analysis of PAPSS2 expression in tumor tissues showed a significant decrease in the bupivacaine-treated group, further confirming the inhibition of melanoma proliferation and metastasis through PAPSS2 suppression. Compared to existing literature, our findings align with re-

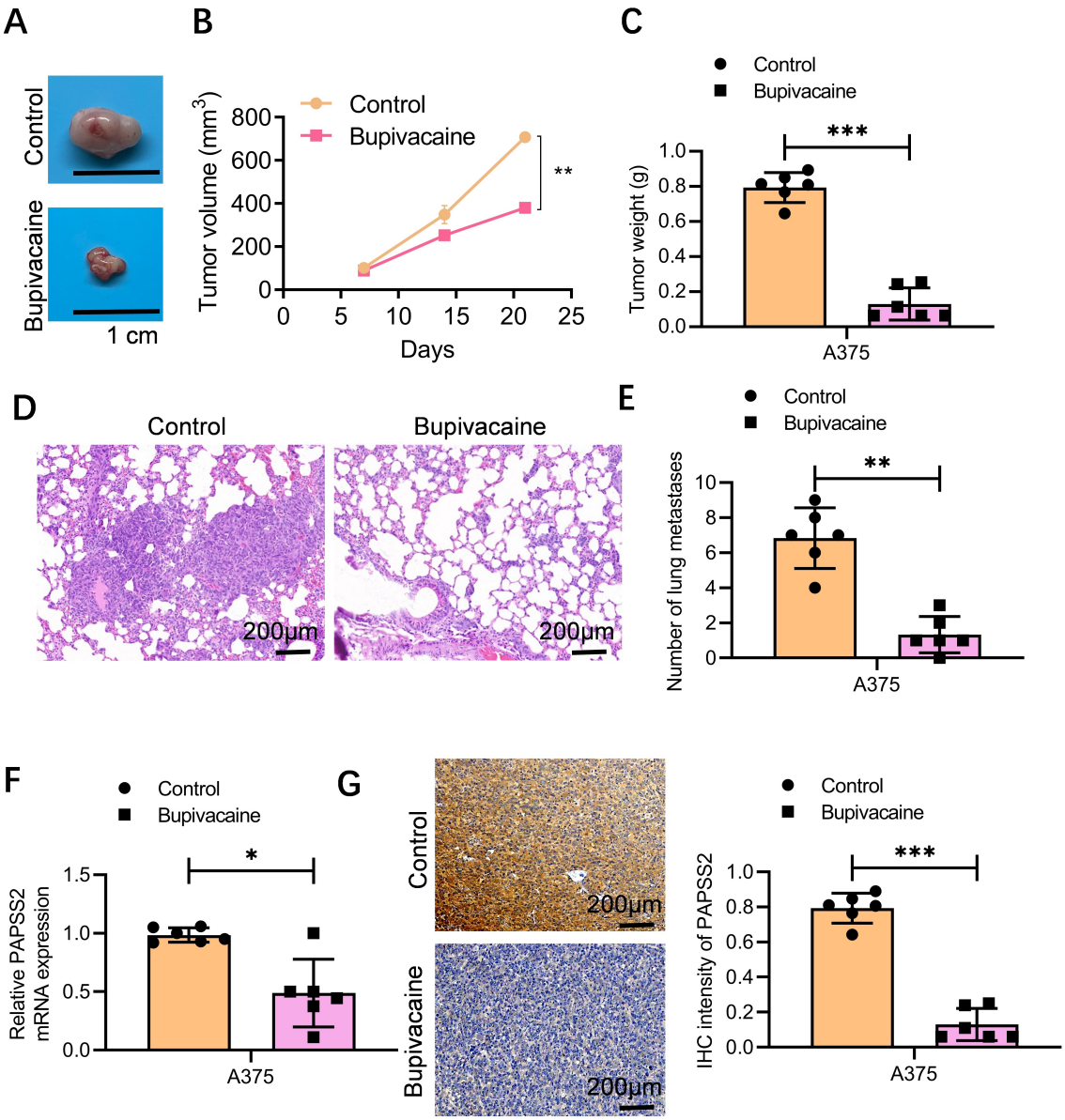

Fig. 7. Bupivacaine inhibits melanoma growth and metastasis via the PAPSS2 signaling pathway. (A,B) Representative images of tumor growth and tumor growth curves in nude mice treated with bupivacaine or control. (C) Tumor weights in nude mice treated with bupivacaine or control. (D) Representative Hematoxylin and Eosin (HE) staining of lung metastasis in nude mice treated with bupivacaine or control. Scale bar = 200 μm. (E) Effect of bupivacaine treatment on tumor metastasis. (F) Quantitative qRT-PCR analysis of *PAPSS2* expression in tumor tissues. (G) Immunohistochemical analysis of PAPSS2 expression in tumor tissues. Scale bar = 200 μm. $*p < 0.05$, $**p < 0.01$, $***p < 0.001$. n = 6.

search conducted by Xuan *et al.* [20], Gu *et al.* [25], and Wang *et al.* [28], which similarly reported bupivacaine's ability to inhibit the proliferation of diverse cancer cells. However, our study is the first to identify that bupivacaine downregulates PAPSS2, a key factor in controlling the malignant behavior of melanoma. Furthermore, research by Zhang *et al.* [18] (2019) demonstrated the close correlation between PAPSS2 expression in breast cancer and prognosis, further confirming the clinical relevance of our findings. This discovery provides a new perspective for the development of novel anti-melanoma strategies, specifically targeting PAPSS2 to inhibit tumor growth and metastasis.

As for the underlying mechanism by which PAPSS2 regulates cancer cell migration, it is important to note that PAPSS2 is primarily known for its role in sulfate metabolism, and its involvement in cancer is not yet fully understood. However, sulfation reactions mediated by enzymes like PAPSS2 can impact various cellular processes,

including cell proliferation, invasion, and migration. One potential mechanism involves the regulation of growth factors and signaling pathways. Sulfation can modify the activity and binding affinity of growth factors, such as transforming growth factor-beta (TGF-beta) and fibroblast growth factor (FGF). These growth factors play crucial roles in cancer cell migration and invasion. Therefore, alterations in sulfate metabolism mediated by PAPSS2 might influence the migratory abilities of cancer cells by modulating the signaling cascades involved. Another possible mechanism involves the sulfation of extracellular matrix (ECM) components. Sulfation of ECM molecules, such as heparan sulfate proteoglycans, can impact cell-matrix interactions and cell migration. PAPSS2 may regulate the sulfation patterns of these ECM molecules, thereby influencing cancer cell migration. To better understand the specific mechanisms involved in the interaction between bupivacaine and PAPSS2, or the underlying mechanism of PAPSS2 in cancer cell migration, further research and investigations specifically addressing these questions are necessary.

Although our study provides a potential mechanism for bupivacaine as an anti-melanoma drug, several limitations remain. First, this study primarily relies on cell and animal models, warranting further validation of its clinical efficacy and safety through future clinical trials. Second, the inhibitory effect of bupivacaine on PAPSS2 may not be the sole mechanism of its anti-tumor effect, as other unidentified molecular targets may be involved. Additionally, due to the heterogeneity of melanoma, the efficacy of bupivacaine on different subtypes of melanoma may vary, which needs to be further explored in future studies. Future research should prioritize identifying the exact molecular mechanisms of bupivacaine in inhibiting PAPSS2, while simultaneously assessing its role across different subtypes and pathological stages of melanoma. Investigating the potential synergistic effects of bupivacaine and other antitumor drugs in combination therapy is also an important direction for future research. Furthermore, research should be expanded to investigate the impact of bupivacaine on the tumor microenvironment, including immune cell infiltration and regulation of tumor-related inflammation, which may provide new strategies for comprehensive melanoma treatment.

Conclusion

In conclusion, the results of this study demonstrate that bupivacaine can significantly inhibit the proliferation and migration ability of melanoma cells. Furthermore, we observed that bupivacaine treatment significantly reduced the expression and activity of PAPSS2, which is closely associated with melanoma proliferation and metastasis. These findings provide new insights into the role of the local anesthetic bupivacaine in inhibiting the proliferation and metastasis of melanoma, laying the foundation for future clinical applications and drug development. Despite inherent limitations, these findings offer promising avenues for melanoma treatment and may have relevance for the treatment of other types of cancer.

Availability of Data and Materials

All experimental data included in this study can be obtained by contacting the corresponding author if needed.

Author Contributions

EJG, JPZ and NX performed the research. EJG and YNL provided help and advice on the experiments. NX, JTZ and YNL contributed to the analysis and interpretation of the data. All authors contributed to the drafting and critical revision of the manuscript. All authors read and approved the final manuscript. All authors have participated sufficiently in the work to take public responsibility for appropriate portions of the content and agreed to be accountable for all aspects of the work in ensuring that questions related to its accuracy or integrity.

Ethics Approval and Consent to Participate

This study was approved by the Committee of Shenzhen Longhua District Central Hospital (No.2021-163-01).

Acknowledgment

Not applicable.

Funding

This research received no external funding.

Conflict of Interest

The authors declare no conflict of interest.

References

[1] Long GV, Swetter SM, Menzies AM, Gershenwald JE, Scolyer RA. Cutaneous melanoma. Lancet. 2023; 402: 485–502.

[2] Saginala K, Barsouk A, Aluru JS, Rawla P, Barsouk A. Epidemiology of Melanoma. Medical Sciences. 2021; 9: 63.

[3] Davis LE, Shalin SC, Tackett AJ. Current state of melanoma diagnosis and treatment. Cancer Biology & Therapy. 2019; 20: 1366–1379.

[4] Jenkins RW, Fisher DE. Treatment of Advanced Melanoma in 2020 and Beyond. The Journal of Investigative Dermatology. 2021; 141: 23–31.

[5] Lugović-Mihić L, Ćesić D, Vuković P, Novak Bilić G, Šitum M, Špoljar S. Melanoma Development: Current Knowledge on Melanoma Pathogenesis. Acta Dermatovenerologica Croatica. 2019; 27: 163–168.

[6] Raimondi S, Suppa M, Gandini S. Melanoma Epidemiology

and Sun Exposure. Acta Dermato-Venereologica. 2020; 100: adv00136.

[7] Teixido C, Castillo P, Martinez-Vila C, Arance A, Alos L. Molecular Markers and Targets in Melanoma. Cells. 2021; 10: 2320.

[8] Atkins MB, Curiel-Lewandrowski C, Fisher DE, Swetter SM, Tsao H, Aguirre-Ghiso JA, *et al*. The State of Melanoma: Emergent Challenges and Opportunities. Clinical Cancer Research. 2021; 27: 2678–2697.

[9] Czarnecka AM, Bartnik E, Fiedorowicz M, Rutkowski P. Targeted Therapy in Melanoma and Mechanisms of Resistance. International Journal of Molecular Sciences. 2020; 21: 4576.

[10] Ralli M, Botticelli A, Visconti IC, Angeletti D, Fiore M, Marchetti P, *et al*. Immunotherapy in the Treatment of Metastatic Melanoma: Current Knowledge and Future Directions. Journal of Immunology Research. 2020; 2020: 9235638.

[11] Albittar AA, Alhalabi O, Glitza Oliva IC. Immunotherapy for Melanoma. Advances in Experimental Medicine and Biology. 2020; 1244: 51–68.

[12] Kuryk L, Bertinato L, Staniszewska M, Pancer K, Wieczorek M, Salmaso S, *et al*. From Conventional Therapies to Immunotherapy: Melanoma Treatment in Review. Cancers. 2020; 12: 3057.

[13] Amaria RN, Menzies AM, Burton EM, Scolyer RA, Tetzlaff MT, Antdbacka R, *et al*. Neoadjuvant systemic therapy in melanoma: recommendations of the International Neoadjuvant Melanoma Consortium. The Lancet. Oncology. 2019; 20: e378–e389.

[14] Seth R, Messersmith H, Kaur V, Kirkwood JM, Kudchadkar R, McQuade JL, *et al*. Systemic Therapy for Melanoma: ASCO Guideline. Journal of Clinical Oncology. 2020; 38: 3947–3970.

[15] Mustafa S, Hussain MF, Latif M, Ijaz M, Asif M, Hassan M, *et al*. A Missense Mutation (c.1037 G > C, p. R346P) in *PAPSS2* Gene Results in Autosomal Recessive form of Brachyolmia Type 1 (Hobaek Form) in A Consanguineous Family. Genes. 2022; 13: 2096.

[16] Noordam C, Dhir V, McNelis JC, Schlereth F, Hanley NA, Krone N, *et al*. Inactivating PAPSS2 mutations in a patient with premature pubarche. The New England Journal of Medicine. 2009; 360: 2310–2318.

[17] Oostdijk W, Idkowiak J, Mueller JW, House PJ, Taylor AE, O'Reilly MW, *et al*. PAPSS2 deficiency causes androgen excess via impaired DHEA sulfation–in vitro and in vivo studies in a family harboring two novel PAPSS2 mutations. The Journal of Clinical Endocrinology and Metabolism. 2015; 100: E672–E680.

[18] Zhang Y, Zou X, Qian W, Weng X, Zhang L, Zhang L, *et al*. Enhanced PAPSS2/VCAN sulfation axis is essential for Snail-mediated breast cancer cell migration and metastasis. Cell Death and Differentiation. 2019; 26: 565–579.

[19] Ibeawuchi C, Schmidt H, Voss R, Titze U, Abbas M, Neumann J, *et al*. Exploring prostate cancer genome reveals simultaneous losses of PTEN, FAS and PAPSS2 in patients with PSA recurrence after radical prostatectomy. International Journal of Molecular Sciences. 2015; 16: 3856–3869.

[20] Xuan W, Zhao H, Hankin J, Chen L, Yao S, Ma D. Local anesthetic bupivacaine induced ovarian and prostate cancer apoptotic cell death and underlying mechanisms in vitro. Scientific Reports. 2016; 6: 26277.

[21] Chahar P, Cummings KC, 3rd. Liposomal bupivacaine: a review of a new bupivacaine formulation. Journal of Pain Research. 2012; 5: 257–264.

[22] Ilfeld BM, Eisenach JC, Gabriel RA. Clinical Effectiveness of Liposomal Bupivacaine Administered by Infiltration or Peripheral Nerve Block to Treat Postoperative Pain. Anesthesiology. 2021; 134: 283–344.

[23] Dan J, Gong X, Li D, Zhu G, Wang L, Li F. Inhibition of gastric cancer by local anesthetic bupivacaine through multiple mechanisms independent of sodium channel blockade. Biomedicine & Pharmacotherapy. 2018; 103: 823–828.

[24] Tam KW, Chen SY, Huang TW, Lin CC, Su CM, Li CL, *et al*. Effect of wound infiltration with ropivacaine or bupivacaine analgesia in breast cancer surgery: A meta-analysis of randomized controlled trials. International Journal of Surgery. 2015; 22: 79–85.

[25] Gu JH, Liu CC, Xie JL, Ma B, Cui SM, Yang GZ, *et al*. The Local Anesthetic Bupivacaine Inhibits the Progression of Non-Small Cell Lung Cancer by Inducing Autophagy Through Akt/mTOR Signaling. Frontiers in Oncology. 2021; 11: 616445.

[26] Gulberti S, Mao X, Bui C, Fournel-Gigleux S. The role of heparan sulfate maturation in cancer: A focus on the 3O-sulfation and the enigmatic 3O-sulfotransferases (HS3STs). Seminars in Cancer Biology. 2020; 62: 68–85.

[27] Marques C, Reis CA, Vivès RR, Magalhães A. Heparan Sulfate Biosynthesis and Sulfation Profiles as Modulators of Cancer Signalling and Progression. Frontiers in Oncology. 2021; 11: 778752.

[28] Wang L, Guo W, Guan H, Yan N, Cai X, Zhu L. Local anesthetic bupivacaine inhibits proliferation and metastasis of hepatocellular carcinoma cells via suppressing PI3K/Akt and MAPK signaling. Journal of Biochemical and Molecular Toxicology. 2021; 35: e22871.